Mon. Not. R. Astron. Soc. **346,** 1103–1115 (2003)

The evolution of $\Omega_{\rm H\,I}$ and the epoch of formation of damped Lyman α absorbers

C. Péroux,[1⋆]† R. G. McMahon,[1]† L. J. Storrie-Lombardi[2]† and M. J. Irwin[1]†
[1]*Institute of Astronomy, Madingley Road, Cambridge CB3 0HA*
[2]*SIRTF Science Center, California Institute of Technology, MS 314-6, Pasadena, CA 91125, USA*

Accepted 2003 August 20. Received 2003 August 19; in original form 2001 May 18

ABSTRACT

We present a study of the evolution of the column density distribution, $f(N, z)$, and total neutral hydrogen mass in high column density quasar absorbers using candidates from a recent high-redshift survey for damped Lyman α (DLA) and Lyman-limit system (LLS) absorbers. The observed number of LLS [$N(\mathrm{H\,I}) > 1.6\times10^{17}$ atom cm^{-2}] is used to constrain $f(N, z)$ below the classical DLA definition of 2×10^{20} atom cm^{-2}. The evolution of the number density of LLS is consistent with our previous work but steeper than previously published work of other authors. At $z = 5$, the number density of Lyman-limit systems per unit redshift is $\sim$5, implying that these systems are a major source of ultraviolet (UV) opacity in the high-redshift Universe. The joint LLS–DLA analysis shows unambiguously that $f(N, z)$ deviates significantly from a single power law and that a Γ-law distribution of the form $f(N, z) = (f_*/N_*)(N/N_*)^{-\beta}\exp(-N/N_*)$ provides a better description of the observations. These results are used to determine the amount of neutral gas contained in DLAs and in systems with lower column density. Whilst in the redshift range 2–3.5, $\sim$90 per cent of the neutral H I mass is in DLAs, we find that at $z > 3.5$ this fraction drops to only 55 per cent and that the remaining 'missing' mass fraction of the neutral gas lies in sub-DLAs with $N(\mathrm{H\,I})$ 10^{19}–2×10^{20} atom cm^{-2}. The characteristic column density, N_*, changes from 1.6×10^{21} atom cm^{-2} at $z < 3.5$ to 2.9×10^{20} atom cm^{-2} at $z > 3.5$, supporting a picture where at $z > 3.5$, we are directly observing the formation of high column density neutral hydrogen DLA systems from lower column density units. Moreover, since current metallicity studies of DLA systems focus on the higher column density systems they may be giving a biased or incomplete view of global galactic chemical evolution at $z > 3$. After correcting the observed mass in H I for the 'missing' neutral gas the comoving mass density now shows no evidence for a decrease above $z = 2$.

Key words: galaxies: evolution – galaxies: formation – intergalactic medium – quasars: absorption lines – cosmology: observations.

1 INTRODUCTION

One of the fundamental phenomena still poorly understood in cosmology is the detailed process relating to the origin of structure formation after the epoch of recombination. The basic dilemma is, that while the directly observable baryonic content of galaxies at the present epoch is concentrated in stars, in the past, logically, this must have been in the form of gas. Therefore, the only way to obtain a self-consistent and complete picture of the galaxy formation process is to combine studies of the starlight and the star formation rate with studies of the gas content of the Universe to learn about the underlying metal production and gas consumption rates.

Quasar absorbers provide a powerful observational means to study the early stages of galaxy formation independent of their intrinsic luminosity. The hydrogen absorbers are normally divided into three classes according to their column density: damped Lyman α (DLA) systems with $N(\mathrm{H\,I}) \geqslant 2\times10^{20}$ atom cm^{-2}; Lyman-limit systems (LLS) with $N(\mathrm{H\,I}) \geqslant 1.6\times10^{17}$ atom cm^{-2}; and the Lyman α forest with $N(\mathrm{H\,I})$ ranging from $\simeq10^{12}$ to 1.6×10^{17} atom cm^{-2}. The damped Lyman α absorption lines are of particular importance since they contain the bulk of the neutral gas in the Universe at high redshift and are the major directly observable baryonic component at these redshifts.

⋆Present address: Osservatorio Astronomico di Trieste, Via Tiepolo, 11, 34 131 Trieste, Italy.
†E-mail: peroux@ts.astro.it (CP); rgm@ast.cam.ac.uk (RGM); lisa@ipac.caltech.edu (LJS-L); mike@ast.cam.ac.uk (MJI)

For historical reasons based on the observed H I column density distribution in local galactic discs, Wolfe et al. (1986) introduced a defining limit for DLAs of $N(\mathrm{H\,I}) \geqslant 2\times10^{20}$ atom cm^{-2}. This definition arises from the fact that 21-cm observations of local spirals show the column density drops sharply beyond this threshold (Bosma 1981). These systems exhibit strong damping wings, however, technically any absorption system with a Doppler parameter $b <$ 100 km s^{-1} and $N(\mathrm{H\,I}) > 10^{19}$ cm^{-2} will exhibit damping wings. As we will show, this 'low-redshift' DLA definition needs to be extended at high redshift to include systems down to 10^{19} atom cm^{-2}.

DLAs were originally thought to be the precursors of present-day L_* disc galaxies (Wolfe et al. 1986), a scenario that is supported by some current models (Prochaska & Wolfe 1998). However, Haehnelt, Steinmetz & Rauch (1998) and Ledoux et al. (1998) have shown that the rotating disc interpretation for DLA systems is not unique and that the velocity structure observed by Wolfe and co-workers can also be explained by infalling subgalactic clumps in collapsing dark matter haloes with virial velocities of $\sim$100 km s^{-1}.

LLS are a lower column density superset of DLAs, which at $z < 1$ are probably associated with galactic haloes (Steidel, Dickinson & Persson 1994). At high-redshift LLS, irrespective of their physical nature, are an important contributor to the ultraviolet (UV) opacity of the Universe since they essentially block all radiation shortward of 912 Å in the rest frame.

In this paper we present an analysis based on a new sample of high column density absorbers (DLA candidates and LLS) from a recently completed high-redshift survey (Péroux et al. 2001) combined with data from the literature (Storrie-Lombardi et al. 1996c; Storrie-Lombardi & Wolfe 2000 and references therein). The combined high-redshift data set is based on observations of $\sim$100 quasars with $z > 4$ and includes complete samples of 29 DLA candidates and 37 LLS with $z > 3.5$. The layout of this paper is as follows. Section 2 shows how the LLS can be used to constrain the cumulative number of absorbers above $\log N(\mathrm{H\,I}) = 17.2$ atom cm^{-2} and examines the redshift evolution of the column density distribution. The cosmological neutral gas evolution is presented in Section 3 and implications of our results on theories of structure formation are detailed in Section 4. Unless otherwise stated, this paper assumes $\Omega_\Lambda = 0.7$, $\Omega_M = 0.3$ and $H_0 = 65$ km s^{-1} Mpc^{-1}.

2 COLUMN DENSITY DISTRIBUTION

Our new sample of high-redshift Lyman-limit systems (Péroux et al. 2001) is combined with data collected from previous surveys (Storrie-Lombardi et al. 1994) in order to determine the number of LLS per unit redshift (Fig. 1). We have chosen to use LLS with $z \geqslant 2.4$ in our analysis because of the very small number of systems known at low redshift ($0.4 \leqslant z \leqslant 2.4$), all of which are below $z = 1.1$. Moreover, the paper is mainly concerned with the evolution of the high column density absorber population at $z > 2$.

In the case of the colour-selected quasars observed by Storrie-Lombardi et al. (1996c) and Péroux et al. (2001), objects with $z < 4.2$ are excluded to minimize colour selection bias. Only LLS with optical depth $\tau > 1$ are used, resulting in 67 systems in 124 quasars without broad absorption features, *not* within 3000 km s^{-1} of the quasar emission redshift. The latter systems are excluded as they might be associated with the quasar itself (Storrie-Lombardi et al. 1994). Details on the LLS selection process and redshift estimates can be found in Péroux et al. (2001). Our new sample adds 26 LLS systems at $z > 3.5$ to the 11 systems used by Storrie-Lombardi et al. (1994). The analysis follows that of Storrie-Lombardi et al. (1994) and the LLS number density is fitted using a power law of the form

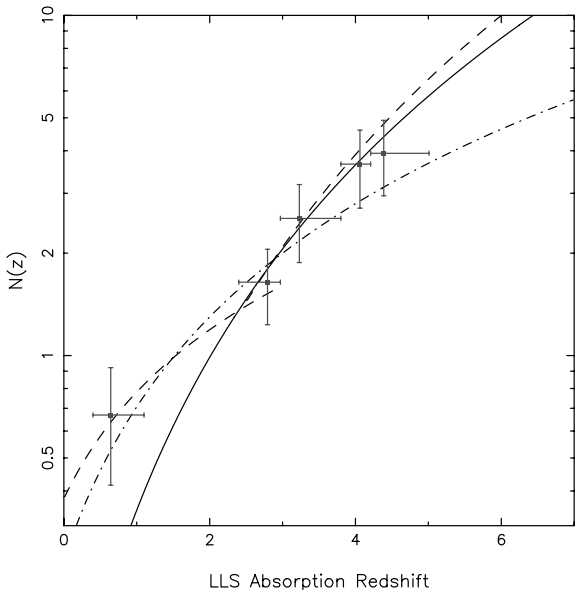

Figure 1. Number of Lyman-limit systems per unit redshift. The solid line is a fit for $z > 2.4$. The dashed lines are the double power-law fits from Storrie-Lombardi et al. (1994) and the dashed-dotted line is the fit from Stengler-Larrea et al. (1995). The horizontal error bars are the bin sizes and the vertical error bars are the 1σ uncertainties. The data are binned for display purposes only.

$N(z) = N_0(1+z)^\gamma$. The parameter values for our fit, $N_0 = 0.07^{+0.13}_{-0.04}$ and $\gamma = 2.45^{+0.75}_{-0.65}$, are determined using a maximum-likelihood analysis. Interestingly, the number density distribution in the Lyman α forest shows a break at $z \sim 1.5$, below which the distribution is flat ($\gamma \sim 0.2$, Weymann et al. 1998) and above which the distribution is steep ($\gamma = 2.19 \pm 0.27$, Kim, Cristiani & D'Odorico 2001), comparable to the LLS results. Our new determination agrees very well with the previous results of Storrie-Lombardi et al. (1994), but there is a significant difference at high redshift when compared with the extrapolated results of Stengler-Larrea et al. (1995). This is not surprising since their analysis contained no data above $z = 3.5$.

We now analyse the combined samples of Lyman-limit systems and confirmed/candidate damped Lyman α systems. The cumulative number of absorbers per unit distance interval for two redshift ranges is presented in Fig. 2. The absorption distance interval, dX (Bahcall & Peebles 1969; Tytler 1987) is used to correct to comoving coordinates and thus depends on the geometry of the Universe since

$$X(z) = \int_0^z (1+z)^2\left[(1+z)^2(1+z\Omega_M) - z(2+z)\Omega_\Lambda\right]^{-1/2}\,\mathrm{d}z. \quad (1)$$

This equation differs from equation (3) in Storrie-Lombardi, Irwin & McMahon (1996a) in that we have included the terms for a non-zero Λ universe. The data with $N(\mathrm{H\,I}) \geqslant 2\times10^{20}$ atom cm^{-2} are DLA candidates taken from our recent high-redshift survey (our observations more than double the redshift path surveyed at $z \gtrsim 3.5$ – see Péroux et al. 2001) and DLAs published by Storrie-Lombardi & Wolfe (2000). The data used for the analysis are tabulated in Appendices A and B.

The power-law fit to the observed number of LLS per unit redshift is used to calculate the *expected number* of LLS systems:

$$\mathrm{LLS}_{\mathrm{expected}} = \sum_{i=1}^{n}\int_{z_{\min}}^{z_{\max}} N_0(1+z)^\gamma\,\mathrm{d}z, \quad (2)$$

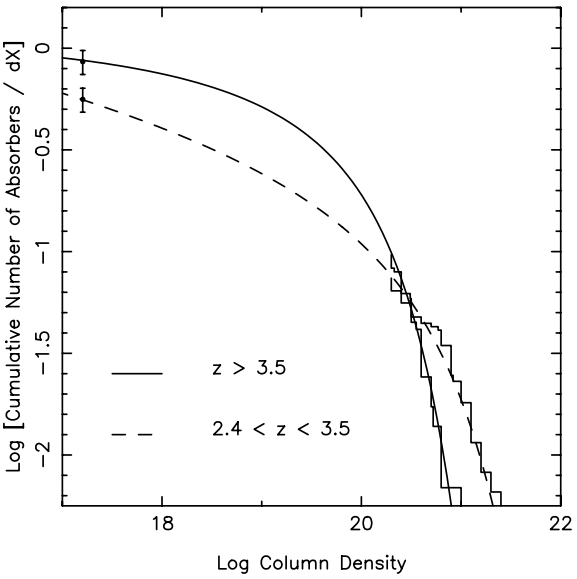

Figure 2. Cumulative number of absorbers per unit distance interval. The data point at log $N(\mathrm{H\,I}) = 17.2$ atom cm^{-2} is the *expected number* of LLS derived from the observed number of LLS per unit redshift. The observations are fitted with a Γ-distribution of the form $f(N, z) = (f_*/N_*)(N/N_*)^{-\beta}\exp(-N/N_*)$.

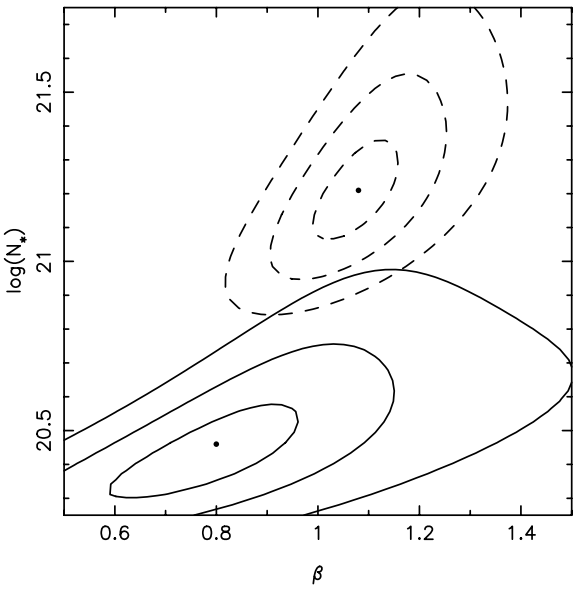

Figure 3. Maximum-likelihood estimator. 1, 2 and 3-σ confidence contours to the Γ-distribution fit of the observed number of absorbers in the redshift range $2.4 < z < 3.5$ (dashed lines) and $z > 3.5$ (solid lines).

where $z_{\rm min}$ and $z_{\rm max}$ define the redshift path along which quasar absorbers were searched for. The LLS line profiles cannot be used to directly measure their column densities because in the range 1.6×10^{17} to 2×10^{20} atom cm^{-2} the curve of growth is degenerate. Nevertheless, the *expected number* of LLS provides a further constraint on the cumulative number of quasar absorbers and clear evidence that a simple power law is *not* a good representation of the observations. We thus choose to fit the data with a Γ-distribution (cf. Schechter 1976, function used in studies of the galaxy luminosity function) as introduced by Pei & Fall (1995) and Storrie-Lombardi, McMahon & Irwin (1996b):

$$f(N, z) = (f_*/N_*)(N/N_*)^{-\beta}\mathrm{e}^{-N/N_*}, \quad (3)$$

where N is the column density, N_* is a characteristic column density and f_* is a normalizing constant. A maximum-likelihood analysis is used to derive the parameters in various redshift ranges (see Table 1). The 1-, 2- and 3σ confidence contours are shown in Fig. 3 for $z < 3.5$ and $z > 3.5$. The distributions are clearly different at the $\sim 3\sigma$ level and indicate that there are fewer high column density systems [$N(\mathrm{H\,I}) > 10^{21}$ atom cm^{-2}] at high redshift, $z > 3.5$, compared with $2 < z < 3.5$, confirming the results from Storrie-Lombardi et al. (1996a) and Storrie-Lombardi & Wolfe (2000). For a comparison with previous works, Fig. 4 shows the column density distribution,

Table 1. Parameter fits to the column density distribution, $f(N, z)$, for absorbers with $\log N(\mathrm{H\,I}) > 17.2$ atom cm^{-2} (see equation 3). N(QSO) is the number of quasars observed and N(DLA) refers to the number of confirmed/candidate damped Lyman α objects detected.

z Range	β	f_* $\times 10^2$	log N_*	N QSO	N DLA	dX	$\Omega_{\rm DLA}$ $\times 10^3$
0.0–2.0	0.74	8.70	20.76	537	23	362.8	0.64
2.0–2.7	1.08	3.25	21.27	380	34	522.3	1.04
2.7–3.5	1.10	4.06	21.18	251	28	414.9	0.98
2.4–3.5	1.08	4.29	21.21	314	46	608.2	1.13
>3.5	0.80	25.1	20.46	112	29	290.2	0.71

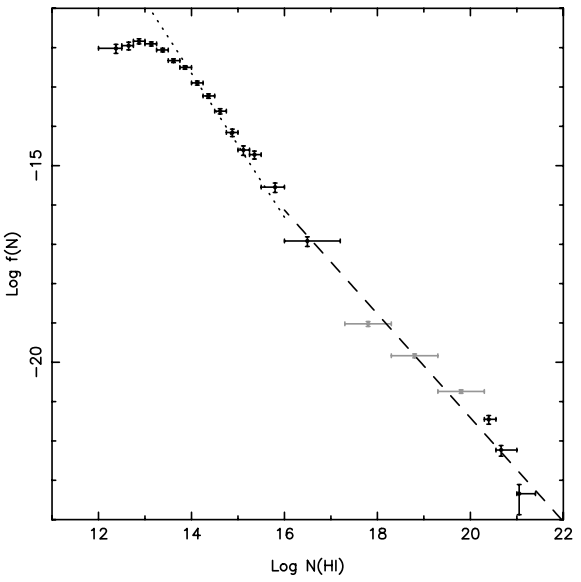

Figure 4. Column density distribution, $f(N, z)$, at $z_{\rm abs} > 3.5$. The low column density data are Keck-HIRES observations of the Lyman α forest (BR 1033−0327 and Q0000−26, Williger et al. 1994; Lu et al. 1996 respectively). The light grey bins [in the range $17.2 < \log N(\mathrm{H\,I}) < 20.3$] are deduced from the fit to the observed cumulative number of quasar absorbers. The turn-over at the low column density end is incompleteness due to a combination of spectral resolution and signal-to-noise ratio. The dashed and dotted lines are the two $\langle z \rangle \simeq 2.8$ power-law fits from Petitjean et al. (1993) corrected for the absorber number density evolution with redshift and to $\Omega_\Lambda = 0.7$, $\Omega_M = 0.3$ cosmology.

$f(N, z)$, at $z_{\rm abs} > 3.5$ together with the double power law of Petitjean et al. (1993).

3 COSMOLOGICAL MASS DENSITY EVOLUTION

The mass density of absorbers can be expressed in units of the current critical mass density, $\rho_{\rm crit}$, as

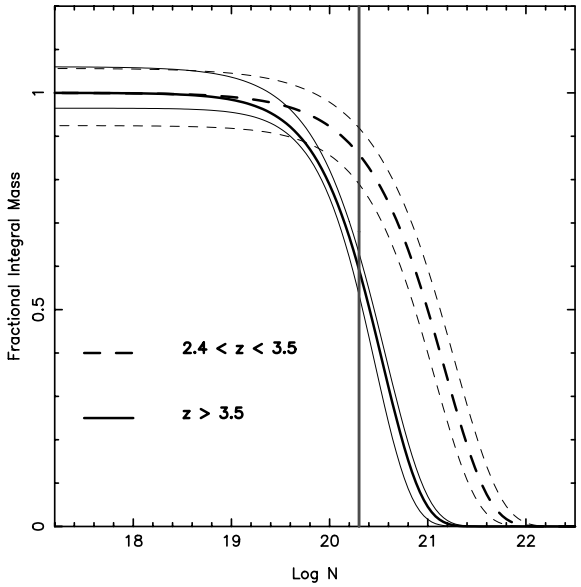

Figure 5. Fractional mass integral plot for two different redshift ranges ($z < 3.5$ and >3.5). The fine lines represent the uncertainties in the model fit. The vertical solid line indicates the boundary of the DLA definition. This plot shows that at $2.4 < z < 3.5$ most of the mass is contained in DLA absorbers with $N(\mathrm{H\,I}) \geqslant 2\times10^{20}$ atom cm^{-2}, while at $z > 3.5$, ~ 45 per cent of the mass is under this formal limit.

$$\Omega_{\mathrm{DLA}}(z) = \frac{H_0 \mu m_{\mathrm{H}}}{c\rho_{\mathrm{crit}}} \int_{N_{\mathrm{min}}}^{\infty} N f(N, z)\, \mathrm{d}N, \quad (4)$$

where μ is the mean molecular weight and m_{H} is the hydrogen mass. The total H I may be estimated as

$$\int_{N_{\mathrm{min}}}^{\infty} N f(N, z)\, \mathrm{d}N = \frac{\sum N_i(\mathrm{HI})}{\Delta X}. \quad (5)$$

If a power law is used to fit $f(N, z)$, up to 90 per cent of the neutral gas is in DLAs (Lanzetta, Wolfe & Turnshek 1995), although an artificial cut-off needs to be introduced at the high column density end because of the divergence of the integral. If instead a Γ-distribution is fitted to $f(N, z)$ this removes the need to artificially truncate the high-end column distribution and can be used to probe in more detail the neutral gas fraction as a function of column density and how this changes with redshift. Fig. 5 shows the cumulative mass fraction as a function of column density for $z>$ and <3.5. At $z \gtrsim 3.5$, up to 45 per cent of the neutral gas is in systems with $10^{19} < N(\mathrm{H\,I}) < 10^{20.3}$. We refer to these systems as *sub-DLAs*. These observations supports a picture where at $z > 3.5$, we are directly observing the formation of high column density neutral hydrogen DLA systems from lower column density units. The value of N_* decreases by a factor of $\approx$5 from 1.6×10^{21} atom cm^{-2} at $z < 3.5$ to 2.9×10^{20} atom cm^{-2} at $z > 3.5$.

Fig. 6 displays Ω_{DLA} contained in DLAs (filled circles) and the total amount of neutral gas (DLAs plus sub-DLAs) for a non-zero Λ universe (grey stars). Our observations are consistent with no evolution in the redshift range $z = 2$–5. Empty universe models produce similar results.

4 DISCUSSION AND CONCLUSIONS

Our study is mainly based on an optically selected quasars, so it is obvious that quasars that lie behind dusty DLA systems will be underrepresented if they exist. Pei & Fall (1995) have used self-consistent closed-box/inflow–outflow galactic chemical evolution models to show that the fraction of missing DLAs at $z = 3$ ranges from 23 to 38 per cent. However, dust is unlikely to be important at high redshift because of the short time available for its production. Dust will have a larger effect at $z = 2$ compared with $z > 3$ and thus it could not cause the form of evolution in $f(N, z)$ that we observe. However, a recent work by Ellison et al. (2001) has shown that measurements of Ω_{DLA} based on optically selected quasar survey are not significantly affected by dust at $z \sim 2$.

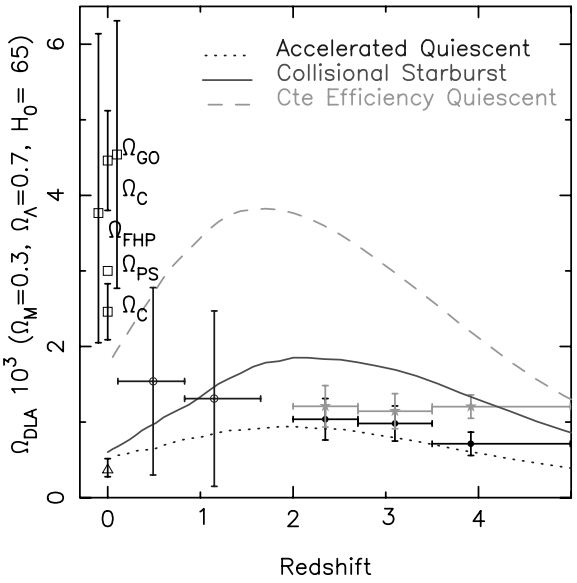

Figure 6. The circles show the neutral gas in damped Lyman α galaxies in a $\Omega_\Lambda = 0.7, \Omega_M = 0.3$ and $h = 0.65$ universe. Vertical error bars correspond to 1σ uncertainties and the horizontal error bars indicate bin sizes. The light grey stars are the total H I + He II including a correction for the neutral gas not contained in DLAs. The open circles at low redshift are the measurements from Rao & Turnshek (2000). The triangle at $z = 0$ is the local H I mass measured by Natarajan & Pettini (1997) who used the most recent galaxy luminosity function to confirm results from Rao & Briggs (1993). The squares, Ω_{FHP}, Ω_{GO}, Ω_{C}, Ω_{PS} (Fukugita, Hogan & Peebles 1998; Gnedin & Ostriker 1992; Cole et al. 2001; Persic & Salucci 1992, respectively) are $\Omega_{\mathrm{stellar}}$ in local galaxies. The error bars for Ω_{C} plotted here do not include uncertainties in the galactic mass-to-light ratio. Semi-analytical models which vary in their recipe for star formation are overplotted (Somerville, Primack & Faber 2001). These represent the cold gas (molecular plus neutral) and thus should lie above the observations.

It is possible that the overall cosmological evolution of Ω_{DLA} is dominated by feedback processes rather than by gas consumption due to star formation. The observed mass of H I at any redshift may relate more to the recombination time-scale for the ionized H II and the time-scale for cooling and collapse into molecular hydrogen (H_2) and thereafter into stars. Models from Efstathiou (2000) indicate that DLA systems might predominantly be due to the outer parts of galaxies that do not even participate in star formation.

It can be seen in Fig. 6 that Ω_{DLA} is significantly below the current estimates of Ω_M in stars in the nearby Universe. This is a significant change in the situation compared with Storrie-Lombardi et al. (1996c) (Fig. 1b). The main reason for this change is that for the currently favoured Λ-dominated cosmology, the mass in H I at high redshift drops by a factor of $\sim$50 per cent compared with an $\Omega_M = 1$ universe. This is purely a geometric effect and mainly affects the relative normalization between $z = 2$ and 0.

In any case, the observations in the redshift range 2–5 show no evolution in the *total* amount of neutral gas in contrast to the earlier results of Lanzetta et al. (1995), who found that $\Omega_{\rm DLA}(z \sim 3)$ was twice $\Omega_{\rm DLA}(z \sim 2)$. Under simple assumptions of closed-box evolution, this could be interpreted as indicating there is little gas consumption due to star formation in DLA systems in this redshift range. Similarly, at $z > 2$, Prochaska, Gawiser & Wolfe (2001) conclude that there is no evolution in the metallicity of DLA systems from column-density-weighted Fe abundance measurements in DLAs. Since metallicity studies focus on the higher column density systems they may be giving a biased or incomplete view of global galactic chemical evolution at $z > 3$. These metallicity evolution results are still very much open to debate as another study by Savaglio (2001) shows that the metallicity content of DLAs and sub-DLAs *does* decrease with redshift when one excludes the highest column density systems [$N(\rm H\,I) > 6 \times 10^{20}$] from the analysis. It is important to note that at $z > 3.5$, 90 per cent of the H I lies below this limit. Moreover, the current practice of using column-density-weighted metallicities neglects the fact that the metallicity observations are biased towards high H I column density systems and hence do not necessarily trace the global metallicity evolution.

The detailed comparison of high-redshift ($z > 2$) observations with lower redshifts is currently quite difficult. In the local Universe 21-cm emission measurements are used to determine the neutral gas mass density. However, direct detections of DLA systems are paradoxically more difficult for several reasons: the observed DLA wavelengths are shifted to the UV requiring *Hubble Space Telescope* observations, the redshift path available per quasar is lower and the number of DLA systems per unit redshift is lower. In fact, the most recent determination of $\Omega_{\rm DLA}$ at $z \sim 1$ by Rao & Turnshek (2000) is higher than the previous estimate by Lanzetta, Wolfe & Turnshek (1995).

Nevertheless, since DLAs are the most directly observable baryonic mass systems at high redshift, their properties are an important constraint for theories of galaxy formation (Kauffmann & Charlot 1994; Kauffmann & Haehnelt 2000). For example, Somerville, Primack & Faber (2001) have used the integrated total neutral gas (H I+He II) to constrain models (Fig. 6) that vary in their recipes for star formation (due to collisional starburst, constant efficiency quiescent star formation or accelerated quiescent star formation). The models take into account the 'cold gas', which includes neutral and molecular gas.

To summarize, we find that at $z > 3.5$ the fraction of neutral gas mass in DLAs above the commonly used Wolfe et al. (1986) DLA definition of $N(\rm H\,I) > 2 \times 10^{20}$ atom cm^{-2} is only 55 per cent compared with ∼90 per cent at $z < 3.5$ and that the remaining fraction of the neutral gas mass lies in systems below this limit, in 'sub-DLAs' with column density $10^{19} < N(\rm H\,I) < 2 \times 10^{20}$ atom cm^{-2}. We also find that the total mass is conserved over the redshift range 2–5. This is strongly indicative that we are observing the assembly of high column density systems from lower column density units and independently of the precise physical nature of damped Lyman α shows that we are observing the epoch of their formation or initial collapse. A systematic study of the kinematic and metallic properties of DLA systems with $z > 3.5$ and $N(\rm H\,I)$ above 10^{19} atom cm^{-2} is an obvious programme for the new generation of echelle spectographs on 8-m class telescopes. It will also be important to directly establish the $N(\rm H\,I)$ column density distribution function below 2×10^{20} atom cm^{-2}. We are currently undertaking such a programme using VLT UVES archival echelle data of high-redshift quasars (Dessauges-Zavadsky et al. 2003; Péroux et al. 2003). The data used for the analysis in this paper are available from http://www.ast.cam.ac.uk/∼quasars.

ACKNOWLEDGMENTS

We thank Bob Carswell, Mike Fall, Sandro D'Odorico, Patrick Petitjean, Max Pettini, Martin Rees, and Joop Schaye for helpful discussions. CP is grateful to PPARC and the Isaac Newton Trust for support and RGM thanks the Royal Society and the Raymond and Beverly Sackler Foundation for support.

REFERENCES

Bahcall J.N., Peebles P.J.E., 1969, ApJ, 156, 7
Black J.H., Chafee F.H., Foltz C.B., 1987, ApJ, 317, 442
Bosma A., 1981, AJ, 86, 1825
Cole S. et al. (the 2dFRGS team), 2001, MNRAS, 326, 255
Dessauges-Zavadsky M., Péroux C., Kim T.-S., D'Odorico S., McMahon G.R., 2003, MNRAS, 345, 447
Efstathiou G., 2000, MNRAS, 317, 697
Ellison S., Yan L., Hook I., Pettini M., Wall J., Shaver P., 2001, A&A, 379, 393
Francis P.J., Hewett P.C., 1993, AJ, 106, 2587
Fukugita M., Hogan C., Peebles P., 1998, ApJ, 503, 518
Fynbo J., Moller P., Thomsen B., 2001, A&A, 374, 443
Gnedin N., Ostriker J., 1992, ApJ, 400, 1
Haehnelt M., Steinmetz M., Rauch M., 1998, ApJ, 495, 647
Jannuzi B. et al., 1998, ApJS, 118, 1
Kauffmann G., Charlot S., 1994, ApJ, 430, 97
Kauffmann G., Haehnelt M., 2000, MNRAS, 311, 576
Kim T.-S., Cristiani S., D'Odorico S., 2001, 373, 757
Lanzetta K., Wolfe A., Turnshek D., 1995, ApJ, 440, 435
Ledoux C., Petitjean P., Bergeron J., Wampler J., Srianand R., 1998, A&A, 337, L51
Lu L., Wolfe A.M., 1994, AJ, 108, 44
Lu L., Wolfe A.M., Turnshek D.A., Lanzetta K.M., 1993, ApJS, 84, 1
Lu L., Sargent W., Womble D., Takada-Hidai M., 1996, ApJ, 472, 509
Meyer D.M., Lanzetta K.M., Wolfe A.M., 1995, ApJ, 451, L13
Natarajan P., Pettini M., 1997, MNRAS, 291, 28
Pei Y., Fall M., 1995, ApJ, 454, 69
Péroux C., Storrie-Lombardi L., McMahon R., Irwin M., Hook I., 2001, AJ, 121, 1799
Péroux C., Dessauges-Zavadsky M., D'Odorico S., Kim T.-S., McMahon G.R., 2003, MNRAS, 345, 480
Persic M., Salucci P., 1992, MNRAS, 258, 14P
Petitjean P., Webb J., Rauch M., Carswell R., Lanzetta K., 1993, MNRAS, 262, 499
Pettini M., Smith L.J., Hunstead R.W., King D.L., 1994, ApJ, 426, 79
Prochaska J., Wolfe A., 1998, ApJ, 507, 113
Prochaska J., Gawiser E., Wolfe A., 2001, ApJ, 551, 99
Rao S., Briggs F., 1993, ApJ, 419, 515
Rao S., Turnshek D., 2000, ApJS, 130, 1
Rauch M., Carswell R.F., Robertson G.G., Shaver P.A., Webb J.K., 1990, MNRAS, 242, 698
Sargent W.L.W., Steidel C.C., Boksenberg A., 1988, ApJ, 334, 22
Sargent W.L.W., Steidel C.C., Boksenberg A., 1989, ApJS, 69, 703
Savaglio S., 2001, in Harwit M., ed., Proc. IAU Symp. 204, The Extragalactic Infrared Background and its Cosmological Implications. Astron. Soc. Pac., San Francisco, p. 307
Savaglio S., D'Odorico S., Moller P., 1994, A&A, 281, 331
Schechter P., 1976, ApJ, 203, 297
Somerville R., Primack J., Faber S., 2001, MNRAS, 320, 504
Steidel C., Dickinson M., Persson S., 1994, ApJ, 437, L75
Stengler-Larrea E. et al., 1995, ApJ, 444, 64

Storrie-Lombardi L., Wolfe A., 2000, ApJ, 543, 552
Storrie-Lombardi L., McMahon R., Irwin M., Hazard C., 1994, ApJ, 427, L13
Storrie-Lombardi L., Irwin M., McMahon R., 1996a, MNRAS, 282, 1330
Storrie-Lombardi L., McMahon R., Irwin M., 1996b, MNRAS, 283, L79
Storrie-Lombardi L., McMahon R., Irwin M., Hazard C., 1996c, ApJ, 468, 121
Turnshek D.A., Wolfe A.M., Lanzetta K.M., Briggs F.H., Cohen R.D., Foltz C.B., Smith H.E., Wilkes B.J., 1989, ApJ, 344, 567
Tytler D., 1987, ApJ, 321, 49
Weymann R. et al., 1998, ApJ, 506, 1
Williger G.M., Carswell R.F., Webb J.K., Boksenberg A., Smith M.G., 1989, MNRAS, 237, 635
Williger G., Baldwin J., Carswell R., Cooke A., Hazard C., Irwin M., McMahon R., Storrie-Lombardi L., 1994, ApJ, 428, 574
Wolfe A., Turnshek D., Smith H., Cohen R., 1986, ApJS, 61, 249
Wolfe A.M., Turnshek D.A., Lanzetta K.M., Lu L., 1993, ApJ, 404, 480
Wolfe A.M., Lanzetta K.M., Foltz C.B., Chaffee F.H., 1995, ApJ, 454, 698

APPENDIX A: THE SAMPLE OF QUASARS WITH CONFIRMED OR CANDIDATE DLA ABSORBERS

Table A1 lists the 114 confirmed or candidate DLA absorbers used in our study, their redshift and H I column densities together with the redshift path surveyed for each quasars. The following corrections to the low redshift sample derived by Lanzetta et al. (1995) have been made: the Q1329+4117 DLA at $z_{\rm abs} = 0.5193$, and the Q2112+059 DLA at $z_{\rm abs} = 0.2039$ have been ruled out (Jannuzi et al. 1998; Fynbo, Moller & Thomsen 2001), while Q0302−223 has a DLA at $z_{\rm abs} = 0.1014$ (Jannuzi et al. 1998).

Table A1. Quasars with confirmed/candidate DLAs.

Quasar	$z_{\rm em}$	$z_{\rm min}$	$z_{\rm max}$	$z_{\rm abs}$	log N(H I)	Ref[a]
Q 0000−2619	4.11	2.389	4.060	3.3901	21.4	5, 13
BR J0006−6208	4.455	2.944	4.400	2.97	20.7	25
				3.20	20.9	25
				3.78	21.0	25
Q 0010−0012	2.15	1.634	2.119	2.0233	20.8	4, 10
Q 0013−0029	2.08	1.634	2.049	1.9730	20.7	4, 11
BR B0019−1522	4.528	2.97	4.473	3.4370	20.92	22, 1
Q 0027+0103	2.29	1.634	2.257	1.9375	20.6	4, 10
BR J0030−5129	4.174	2.304	4.122	2.45	20.8	25
Q 0042−2930	2.39	1.591	2.354	1.931	20.5	4
Q 0049−2820	2.26	1.638	2.223	2.0713	20.5	4, 11
Q 0056+0125	3.16	2.197	3.119	2.7750	21.0	4, 10
Q 0058−2914	3.07	1.778	3.052	2.6711	21.2	21
Q 0100−3105	2.64	1.687	2.605	2.131	20.5	4
Q 0100+1300	2.69	1.64	2.74	2.3093	21.4	16, 15
Q 0102−1902	3.04	2.044	2.995	2.3693	21.0	5, 8
Q 0102−0214	1.98	1.649	1.949	1.7431	20.6	4, 10
PSS J0106+2601	4.309	2.764	4.256	3.96	20.5	25
BRI B0111−2819	4.30	2.709	4.247	3.1043	21.0	1
Q 0112−3041	2.99	1.881	2.945	2.4191	20.5	21, 9
Q 0112−3041	2.99	1.881	2.945	2.7023	20.3	21, 9
Q 0112+0300	2.81	1.813	2.785	2.4227	21.0	5, 11
PSS J0132+1341	4.147	2.844	4.096	3.93	20.3	1
PSS J0133+0400	4.154	2.865	4.102	3.69	20.4	25
				3.77	20.5	25
PSS J0134+3307	4.532	2.562	4.477	3.76	20.6	25
Q 0149+3335	2.43	1.64	2.43	2.1413	20.5	16, 7
PSS J0152+0735	4.051	1.890	4.000	3.84	20.7	25
Q 0201+3634	2.49	1.632	2.879	2.4614	20.4	21, 8
Q 0201+3634	2.49	1.632	2.879	1.768	20.5	21
PSS J0209+0517	4.174	2.759	4.122	3.66	20.3	25
				3.86	20.6	25
Q 0216+0803	3.00	1.731	2.953	2.2930	20.5	5, 9
BR J0301−5537	4.133	2.825	4.082	3.22	20.3	25
Q 0302−223	1.4000	1.0077	1.3760	1.0104	20.36	24
BR J0307−4945	4.728	3.138	4.671	4.46	20.8	25
SDSS J0310−0014	4.658	3.087	4.601	3.42	20.5	25
BR B0331−1622	4.38	2.868	4.326	3.56	20.6	1
BR J0334−1612	4.363	3.080	4.309	3.56	21.0	25
Q 0336−0142	3.20	2.109	3.155	3.0619	21.2	21, 8
SDSS J0338+0021	5.010	3.528	4.950	4.06	20.4	25
Q 0347−3819	3.23	2.044	3.186	3.0244	20.8	21, 18
BR J0426−2202	4.320	2.544	4.267	2.98	21.1	25
Q 0449−1330	3.097	2.006	3.056	2.052	20.4	21

Table A1 – *continued*

Quasar	$z_{\rm em}$	$z_{\rm min}$	$z_{\rm max}$	$z_{\rm abs}$	log N(H I)	Ref[a]
Q 0458−0203	2.29	1.96	2.29	2.0399	21.7	16, 7
Q 0528−2505	2.779	1.961	2.741	2.1404	21.0	5
PSS J0747+4434	4.430	2.764	4.376	3.76	20.3	25
				4.02	20.6	25
Q 0834−2006	2.75	1.632	2.704	1.715	20.4	21
Q 0836+1122	2.70	1.74	2.67	2.4660	20.6	16, 6
Q 0913+0715	2.78	1.866	2.739	2.6187	20.3	21, 8
MG 0930+2858	3.41	2.173	3.366	3.24	20.5	2
Q 0935+4143	1.9800	1.0626	1.550	1.369	20.3	3
BR B0951−0450	4.369	2.93	4.315	3.8580	20.6	22, 1
BR B0951−0450	4.369	2.93	4.315	4.2028	20.4	22, 1
BRI B0952−0115	4.426	2.99	4.372	4.0238	20.55	22, 1
PC 0953+4749	4.457	3.010	4.004	3.403	20.9	1
PC 0953+4749	4.457	3.010	4.004	3.890	21.1	1
BRI B1013+0035	4.405	2.61	4.351	3.1031	21.1	22, 1
Q 1032+0414	3.39	2.067	3.347	2.839	20.3	21
PSS J1057+4555	4.116	2.652	4.065	3.05	20.3	1, 25
BRI B1108−0747	3.922	2.64	3.873	3.607	20.33	22, 23
BRI B1114−0822	4.495	3.19	4.440	4.2576	20.3	22, 1
Q 1151+0651	2.76	1.65	2.76	1.7737	21.3	16, 6
Q 1159+0132	3.27	1.988	3.226	2.6846	21.1	21, 8
PSS J1159+1337	4.073	2.563	4.022	3.72	20.3	25
BR B1202−0725	4.694	3.16	4.637	4.383	20.49	22, 23
Q 1205+0918	2.08	1.634	2.046	1.673	20.6	4
Q 1209+0919	3.30	2.175	3.254	2.5835	21.4	21, 8
Q 1210+1731	2.54	1.634	2.502	1.8920	20.6	4, 10
Q 1215+3322	2.61	1.64	2.60	1.9989	21.0	16, 7
Q 1223+1753	2.92	1.945	2.879	2.4658	21.5	4, 11
Q 1232+0815	2.57	1.789	2.534	2.3376	20.9	4, 10
Q 1240+1516	2.28	1.634	2.247	1.738	20.7	4
Q 1244+3443	2.48	1.64	2.50	1.8593	20.5	16, 7
Q 1246−0217	2.11	1.634	2.075	1.779	21.2	4
PSS J1253−0228	4.007	2.498	3.957	2.78	21.4	25
Q 1308+0105	2.80	1.634	2.763	1.762	20.6	4
GB 1320+3927	2.98	1.968	2.940	2.11	20.4	2
Q 1337+1121	2.92	1.86	2.92	2.7957	20.9	16, 6
BRI B1346−0322	3.992	2.65	3.942	3.7343	20.72	22, 1
Q 1347+1116	2.70	1.92	2.71	2.4709	20.3	16, 6
Q 1409+0930	2.86	1.979	2.800	2.4561	20.5	21, 8
PSS J1443+2724	4.407	2.950	4.353	4.216	20.8	1
Q 1451+1223	3.26	2.158	3.207	2.478	20.4	16, 21
BR BI1500+0824	3.943	2.39	3.894	2.7968	20.8	22, 1
GB 1610+2806	3.54	2.021	3.498	2.59	20.6	2
MG 1614+0506	3.21	1.984	3.168	2.52	20.4	2
PSS J1618+4125	4.213	2.820	4.161	3.92	20.5	25
RX J1759+6638	4.320	2.804	4.267	3.40	20.4	25
GB 1759+7539	3.05	1.955	3.010	2.624	20.77	2
PSS J1802+5616	4.158	2.891	4.106	3.76	20.4	25
PC 2047+0123	3.799	2.620	3.751	2.7299	20.4	1
PSS J2122−0014	4.114	2.350	4.063	3.20	20.3	25
Q 2132−4321	2.42	1.595	2.386	1.916	20.7	4
Q 2138−4427	3.17	2.107	3.128	2.851	20.9	4, 12
PSS J2154+0335	4.363	2.979	4.309	3.61	20.4	25
PSS J2155+1358	4.256	2.940	4.203	3.32	21.1	25
Q 2206−1958	2.56	1.85	2.58	1.9205	20.5	16, 14
Q 2206−1958	2.56	1.85	2.58	2.0763	20.7	16, 17
Q 2223−0512	1.4040	0.4159	0.6310	0.4925	20.9	3
Q 2223−0512	1.4040	0.9259	1.3800			3
Q 2230+0232	2.15	1.634	2.119	1.8642	20.8	4, 10, 11
Q 2231−0015	3.015	1.749	2.980	2.0657	20.6	4, 9
BR B2237−0607	4.558	2.96	4.502	4.0691	20.5	22, 1
Q 2239−3836	3.55	2.389	3.508	3.2810	20.8	21, 9
PSS J2241+1352	4.441	3.027	4.387	4.28	20.7	25

Table A1 – *continued*

Quasar	z_{em}	z_{min}	z_{max}	z_{abs}	log N(H I)	Ref[a]
Q 2248+0127	2.56	1.634	2.524	1.9080	20.6	4, 10
BR J2317−4345	3.943	2.448	3.894	3.49	20.9	25
PSS J2344+0342	4.239	2.696	4.187	3.21	20.9	25
Q 2348−0108	3.01	2.044	2.965	2.4272	20.5	16, 6
Q 2348−0108	3.01	2.044	2.965	2.6161	21.3	21, 6
Q 2351+0217	2.03	1.634	2.000	1.766	20.9	4, 10
Q 2359−0216	2.31	1.747	2.779	2.0951	20.7	16, 7
Q 2359−0216	2.31	1.747	2.779	2.1537	20.3	16, 7

[a]References: (1) Storrie-Lombardi & Wolfe (2000); (2) Storrie-Lombardi & Hook (in preparation); (3) Lanzetta et al. (1995); (4) Wolfe et al. (1995); (5) Sargent, Steidel & Boksenberg (1989); (6) Turnshek et al. (1989); (7) Wolfe et al. (1993); (8) Lu et al. (1993); (9) Lu & Wolfe (1994); (10) Virgilio et al. (private communication); (11) Pettini et al. (1994); (12) Francis & Hewett (1993); (13) Savaglio, D'Odorico & Moller (1994); (14) Sargent, Steidel & Boksenberg (1988); (15) Black, Chaffee & Foltz (1987); (16) Wolfe et al. (1986); (17) Wolfe (private communication); (18) Rauch et al. (1990); (19) Williger et al. (1989); (20) Meyer, Lanzetta & Wolfe (1995); (21) Lanzetta et al. (1991); (22) Storrie-Lombardi et al. (1996c); (23) Storrie-Lombardi et al. (1996a); (24) Jannuzi et al. (1998); (25) Péroux et al. (2001).

APPENDIX B: THE SAMPLE OF QUASARS WITHOUT DLA ABSORBERS

Table B1 lists the quasars from our study where no DLAs where discovered. The table also provides the redshift path surveyed for each quasars.

Table B1. Quasars without DLAs detected.

Quasar	z_{em}	z_{min}	z_{max}	Ref[a]
Q 0001+0842	3.241	2.024	3.229	21
Q 0002+151	1.8990	0.4723	0.6034	3
Q 0002+151	1.8990	1.1198	1.5500	3
Q 0003+158	0.4500	0.0080	0.4355	3
PSS J0003+2730	4.240	2.718	4.188	26
MG 0004+1359	3.25	1.899	3.207	2
Q 0004+1711	2.898	2.002	2.851	21
Q 0006+0230	2.09	1.787	2.059	4
Q 0006+0200	2.35	1.634	2.317	4
Q 0007−0004	2.26	1.634	2.227	4
Q 0007−000	2.29	1.670	2.260	16
MG 0007+0141	2.90	1.882	2.861	2
Q 0007+106	0.0890	0.0080	0.0781	3
Q 0009−0138	1.99	1.634	1.960	4
Q 0009+0219	2.66	1.784	2.623	4
Q 0009−0215	2.11	1.634	2.079	4
Q 0014+8118	3.380	1.928	3.340	21
Q 0014−0256	1.85	1.729	1.821	4
Q 0015+0239	2.47	1.784	2.435	4
Q 0016+0045	2.31	1.651	2.277	4
Q 0018−0220	2.56	1.634	2.524	4
Q 0018+0047	1.83	1.655	1.802	4
Q 0020+0217	1.80	1.665	1.772	4
Q 0022+0150	2.77	1.791	2.732	4
Q 0023+0010	1.90	1.657	1.871	4
Q 0025−0151	2.08	1.634	2.049	4
Q 0026+0158	1.89	1.727	1.861	4
Q 0026+129	0.1420	0.0080	0.1306	3
Q 0027+0149	2.33	1.694	2.297	4
Q 0028+0236	2.00	1.634	1.970	4
Q 0028−0148	2.08	1.840	2.049	4
Q 0029+0017	2.23	1.725	2.198	4
Q 0029−0152	2.39	2.013	2.356	4

Table B1 – *continued*

Quasar	z_{em}	z_{min}	z_{max}	Ref[a]
PSS J0030+1702	4.282	2.763	4.229	1
PSS J0034+1639	4.293	2.981	4.240	26
SDSS J0035+0040	4.747	3.309	4.690	26
Q 0037−018	2.34	1.654	2.303	16
Q 0039−2630	1.81	1.634	1.782	4
Q 0040−2917	2.09	1.634	2.056	4
Q 0041−2638	3.045	1.657	3.029	21
Q 0041−2707	2.79	1.668	2.748	4
Q 0041−2607	2.79	1.634	2.470	4
Q 0041−2658	2.46	1.634	2.422	4
Q 0041−2859	2.13	1.589	2.103	4
Q 0042−3053	1.97	1.634	1.944	4
Q 0042−2627	3.298	2.113	3.253	21
Q 0042−2656	3.33	2.215	3.314	21
Q 0042−2657	2.90	2.226	2.859	4
Q 0043−2937	2.23	1.656	2.198	4
Q 0044+030	0.6240	0.3386	0.6078	3
Q 0045−3002	2.02	1.603	1.991	4
Q 0045−0341	3.138	1.961	3.094	21
Q 0045−013	2.53	1.784	2.493	16
Q 0046−293	4.014	2.882	3.964	1
BRI B0046−2458	4.15	2.575	4.099	1
Q 0047−2759	2.13	1.649	2.099	4
Q 0047−3050	2.97	1.930	2.933	4
Q 0047−2538	1.97	1.591	1.939	4
Q 0047−2326	3.422	2.291	3.378	21
Q 0048−0119	1.88	1.634	1.849	4
Q 0048−2545	2.08	1.634	2.051	4
Q 0049−0104	2.10	1.715	2.065	4
Q 0049−0012	1.95	1.634	1.916	4
Q 0049+007	2.27	1.644	2.238	16
Q 0049+014	2.31	1.681	2.276	16
Q 0049+171	0.0640	0.0080	0.0534	3
Q 0050+124	0.0611	0.0080	0.0505	3
Q 0050−2523	2.16	1.592	2.127	4
Q 0051−0226	2.53	1.634	2.491	4
Q 0052−0058	2.21	1.634	2.180	4
Q 0052+251	0.1550	0.0080	0.1435	3
Q 0053−0134	2.06	1.634	2.031	4
Q 0053−2824	3.616	2.454	3.576	21
Q 0054+0200	1.87	1.634	1.844	4

Table B1 – *continued*

Quasar	$z_{\rm em}$	$z_{\rm min}$	$z_{\rm max}$	Ref[a]
Q 0054+144	0.1710	0.0080	0.1593	3
Q 0054−006	2.76	1.854	2.724	16
Q 0055+0141	2.23	1.651	2.200	4
Q 0055−2744	2.20	1.567	2.163	4
Q 0055−2629	3.6560	1.920	3.609	21
Q 0055−0200	1.98	1.782	1.953	4
Q 0055+0025	1.91	1.634	1.885	4
Q 0056−0241	2.23	1.779	2.194	4
Q 0057−0225	2.01	1.715	1.979	4
Q 0057−274	3.52	2.603	3.475	1
Q 0058−2604	2.47	1.606	2.437	4
Q 0058−0227	2.23	1.712	2.194	4
Q 0058+0155	1.95	1.634	1.924	4
Q 0059−0207	2.29	1.653	2.257	4
Q 0059−2625	2.10	1.614	2.069	4
Q 0059+0035	2.55	1.673	2.510	4
PSS J0059+0003	4.16	2.750	4.108	1
Q 0100+0146	1.91	1.692	1.880	4
Q 0101−2548	1.97	1.596	1.943	4
Q 0101−3025	4.073	1.937	3.116	21
Q 0102−0240	1.84	1.731	1.818	4
BRI B0103+0032	4.437	2.87	4.383	22
Q 0103−0141	2.21	1.634	2.174	4
Q 0103−2901	2.87	1.922	2.831	4
Q 0104+0030	1.87	1.667	1.845	4
PC 0104+0215	4.171	2.881	4.119	1
Q 0105−2649	2.46	1.667	2.428	4
Q 0106−0230	2.28	1.634	2.246	4
Q 0106+0119	2.10	1.871	2.068	4
Q 0107+0022	1.97	1.634	1.938	4
Q 0108+0028	2.01	1.733	1.975	4
Q 0109+022	2.35	1.734	2.317	16
Q 0110−0107	1.89	1.643	1.860	4
Q 0112−2728	2.894	1.784	2.855	21
Q 0114−0856	3.163	1.838	3.118	21
Q 0115−3002	3.249	1.733	3.207	21
PSS J0117+1552	4.244	2.646	4.192	1
Q 0117+213	1.4930	0.9989	1.4681	3
Q 0119−286	0.1170	0.0080	0.1058	3
Q 0119−013	0.0540	0.0080	0.0435	3
Q 0123+257	2.37	1.644	2.338	16
PC 0131+0120	3.792	3.116	3.744	1
PSS J0131+0633	4.417	3.014	4.363	26
Q 0132−1947	3.130	1.714	3.089	21
Q 0134+329	0.3670	0.0080	0.1050	3
BRI B0135−4239	3.97	2.575	3.920	1
Q 0136+010	2.35	1.749	2.317	16
Q 0136+1737	2.73	1.632	2.679	21
Q 0143−0135	3.141	1.673	3.097	21
GB 0148+2502	3.10	1.825	3.059	2
Q 0148−0946	2.850	1.797	2.810	21
BRI B0151−0025	4.194	2.74	4.142	22
Q 0153+0430	2.993	1.673	2.951	21
Q 0157+001	0.1631	0.0080	0.1515	3
Q 0159+036	2.47	1.644	2.436	16
Q 0205+024	0.1564	0.0080	0.1448	3
Q 0207−0019	2.853	1.756	2.817	21
SDSS J0211−0009	4.874	3.402	4.815	26
Q 0215+015	1.7150	0.9996	1.5500	3
Q 0219+428	0.4440	0.0080	0.4296	3
GB 0229+1309	2.07	1.767	2.039	2
Q 0232−042	1.4360	0.0080	0.6320	3
Q 0232−042	1.4360	0.8733	1.4116	3
BR J0234−1806	4.301	2.971	4.248	26

Table B1 – *continued*

Quasar	$z_{\rm em}$	$z_{\rm min}$	$z_{\rm max}$	Ref[a]
Q 0237−233	2.2230	1.1593	1.5402	3
Q 0239−1527	2.786	1.928	2.744	21
BRI B0241−0146	4.053	2.86	4.002	22
BR B0245−0608	4.238	2.96	4.186	22
PSS J0248+1802	4.422	2.810	4.368	1, 26
Q 0249−1826	3.210	1.871	3.163	21
Q 0249−2212	3.21	2.044	3.160	5, 1
Q 0252+0136	2.47	1.634	2.430	4
Q 0254+0000	2.25	1.634	2.215	4
Q 0256−0000	3.377	2.241	3.330	21
Q 0256−0031	2.00	1.634	1.965	4
Q 0258+0210	2.52	1.634	2.489	4
Q 0301−0035	3.226	2.060	3.181	21
Q 0302−0019	3.290	1.739	3.243	21
Q 0305+0127	2.15	1.634	2.118	4
Q 0307−0058	2.11	1.634	2.075	4
Q 0308+0129	2.34	1.739	2.302	4
Q 0308+1902	2.839	1.673	2.797	21
Q 0308−1920	2.756	1.673	2.714	21
BR J0311−1722	4.039	2.591	3.989	26
Q 0312−770	0.2230	0.0080	0.2108	3
Q 0316−2023	2.869	1.747	2.826	21
Q 0323+022	0.1470	0.0080	0.1295	3
BR J0324−2918	4.622	2.900	4.566	26
Q 0329−2534	2.689	1.661	2.662	21
Q 0334−2029	3.132	2.057	3.089	21
PC 0345+0130	3.638	2.699	3.592	1
BR B0351−1034	4.351	3.09	4.297	22
Q 0351−3904	3.01	1.632	2.970	21
Q 0352−2732	2.823	1.673	2.781	21
BR J0355−3811	4.545	3.030	4.490	26
BR B0401−1711	4.236	2.82	4.184	22
BR J0403−1703	4.227	2.992	4.175	26
Q 0405−123	0.5740	0.0080	0.5583	3
Q 0414−060	0.7810	0.0080	0.7632	3
BR J0415−4357	4.070	2.813	4.019	26
BR J0419−5716	4.461	2.820	4.406	26
Q 0420+007	2.918	1.673	2.879	21
Q 0420−3851	3.1230	2.094	3.082	21
BR J0426−2202	4.320	2.544	4.267	26
Q 0428−1342	3.244	1.965	3.200	21
Q 0454−220	0.5340	0.1199	0.5187	3
Q 0454+039	1.3450	0.9672	1.3216	3
Q 0457+024	2.38	1.645	2.346	16
MG 0504+0303	2.46	1.803	2.425	2
Q 0521−365	0.0566	0.0080	0.0460	3
PMN J0525−3343	4.383	2.829	4.329	26
BR J0529−3526	4.413	3.023	4.359	26
BR J0529−3552	4.172	2.821	4.120	26
Q 0537−441	0.8940	0.5139	0.6300	3
Q 0548−322	0.0690	0.0080	0.0583	3
Q 0552+398	2.36	1.644	2.325	16
Q 0558−504	0.1370	0.0080	0.1256	3
Q 0624+691	0.3700	0.0080	0.3563	3
Q 0636+6801	3.178	2.019	3.132	21
Q 0637−752	0.6560	0.0080	0.6251	3
Q 0642+4454	3.408	2.192	3.362	21
Q 0702+646	0.0795	0.0080	0.0687	3
BR J0714−6455	4.462	3.050	4.407	26
Q 0731+6519	3.038	2.019	2.993	21
Q 0735+178	0.4240	0.0765	0.4098	3
Q 0736+017	0.1910	0.0080	0.1791	3
Q 0742+318	0.4620	0.0080	0.4474	3
Q 0743−673	1.5130	1.0302	1.4879	3

Table B1 – *continued*

Quasar	z_{em}	z_{min}	z_{max}	Ref[a]
GB 0749+4239	3.59	2.185	3.544	2
PC 0751+5623	4.281	3.526	4.228	1
Q 0754+100	0.6700	0.0080	0.6257	3
Q 0754+394	0.0958	0.0080	0.0848	3
Q 0804+761	0.1000	0.0080	0.0890	3
Q 0805+0441	2.880	1.838	2.834	21
Q 0812+332	2.42	1.677	2.385	16
Q 0819−032	2.35	1.704	2.319	16
Q 0820+296	2.37	1.644	2.333	16
MG 0830+1009	3.75	2.040	3.703	2
Q 0830+1133	2.979	1.797	2.936	21
Q 0831+1238	2.748	1.961	2.706	21
Q 0837−120	0.1980	0.0080	0.1860	3
Q 0844+349	0.0640	0.0080	0.0534	3
Q 0846+152	2.64	1.831	2.599	16
MG 0848+1533	2.01	1.735	1.980	2
Q 0849+080	0.0620	0.0080	0.0514	3
Q 0851+202	0.3060	0.0080	0.2929	3
Q 0855+182	2.62	1.682	2.580	16
Q 0903+155	2.68	1.659	2.645	16
MG 0906+0406	3.20	1.811	3.158	2
Q 0906+484	0.1180	0.0080	0.1068	3
Q 0910+403	0.9360	0.0080	0.9166	3
Q 0914−621	0.0573	0.0080	0.0467	3
Q 0916+555	0.1235	0.0080	0.1123	3
Q 0932+3646	2.84	1.634	2.814	21
Q 0933+733	2.53	1.651	2.493	16
Q 0938+1159	3.19	1.634	3.149	21
Q 0941+2608	2.913	1.731	2.867	21
Q 0953+414	0.2390	0.0080	0.2266	3
Q 0955+326	0.5330	0.0080	0.5177	3
Q 0956+1217	3.306	2.159	3.263	21
Q 0957+561	1.4050	0.8179	1.3810	3
Q 0958+551	1.7324	1.1762	1.4513	3
Q 1001+291	0.3290	0.0080	0.3157	3
Q 1004+130	0.2410	0.0080	0.2286	3
Q 1004+1411	2.707	1.786	2.672	21
Q 1007+417	0.6110	0.0080	0.5949	3
Q 1009−0252	2.75	1.651	2.708	4
Q 1011−282	0.6110	0.0080	0.1310	3
Q 1011−0144	2.24	1.669	2.204	4
Q 1011+250	1.6310	0.9718	1.5500	3
Q 1012+008	0.1850	0.0080	0.1732	3
Q 1012−0206	2.14	1.634	2.104	4
GB 1013+2052	3.11	1.945	3.069	2
Q 1014+0023	2.29	1.634	2.591	4
Q 1016−0039	2.18	1.649	2.144	4
Q 1017+1055	3.158	2.114	3.127	21
Q 1017+280	1.9280	0.9971	1.4678	3
Q 1018−0005	2.60	1.789	2.560	4
Q 1020+0028	1.90	1.680	1.872	4
Q 1021−0037	2.547	1.887	2.513	21
Q 1024+0030	2.17	1.717	2.135	4
Q 1025−0030	2.87	1.885	2.833	4
RX J1028−0844	4.276	2.533	4.223	26
Q 1028+313	0.1770	0.0080	0.1652	3
Q 1029−140	0.0860	0.0080	0.0751	3
Q 1033+1342	3.07	1.800	3.048	21
BR B1033−0327	4.509	2.91	4.454	22, 23
Q 1038+528	2.30	1.677	2.262	16
GB 1041+3014	2.99	1.735	2.950	2
Q 1047+550	2.1650	1.3299	1.5159	3
BRI B1050−0000	4.286	2.83	4.233	22

Table B1 – *continued*

Quasar	z_{em}	z_{min}	z_{max}	Ref[a]
Q 1100+772	0.3110	0.0080	0.2979	3
Q 1100−264	2.1450	1.1551	1.5500	3
MG 1101+0248	2.51	1.736	2.475	2
Q 1103−006	0.4260	0.0080	0.4117	3
BRI B1110+0106	3.918	2.58	3.869	22
Q 1115+080	1.7180	0.4066	0.6330	3
Q 1115+080	1.7180	0.9595	1.5500	3
Q 1116+215	0.1770	0.0080	0.1652	3
Q 1123+264	2.35	1.645	2.317	16
Q 1124+5706	2.890	1.762	2.851	21
Q 1127+078	2.66	1.644	2.621	16
Q 1128+105	2.65	2.040	2.610	16
Q 1131−0043	2.16	1.653	2.128	4
Q 1132−0054	2.76	1.717	2.718	4
Q 1135−0255	2.41	1.739	2.373	4
Q 1136−135	0.5570	0.0080	0.5414	3
Q 1136+122	2.90	1.781	2.862	16
Q 1137+660	0.6460	0.0080	0.6295	3
Q 1138−0107	2.76	1.953	2.718	4
Q 1139−0139	1.93	1.634	1.884	4
Q 1139−0037	1.91	1.634	1.896	4
Q 1142+0138	2.42	1.791	2.390	4
Q 1142+1015	3.152	2.127	3.109	21
Q 1143+0142	2.28	1.634	2.248	4
Q 1143+099	2.60	1.676	2.567	16
Q 1144+115	2.51	1.682	2.471	16
Q 1144+0140	2.59	1.667	2.551	4
Q 1145−0039	1.94	1.634	1.912	4
Q 1145+0121	2.08	1.721	2.045	4
Q 1146+0207	2.06	1.634	2.025	4
Q 1147+084	2.61	1.854	2.577	16
GB 1147+4348	3.02	2.035	2.980	2
Q 1148−0007	1.977	1.634	1.947	4
Q 1148+0055	1.89	1.667	1.858	4
Q 1148+549	0.9690	0.0080	0.9493	3
Q 1151+117	0.1760	0.0080	0.1642	3
Q 1156+295	0.7290	0.0080	0.7117	3
Q 1159+0039	2.586	1.671	2.550	21
Q 1202+281	0.1650	0.0080	0.1534	3
Q 1205−3014	3.036	2.045	2.996	21
Q 1206+1155	3.106	2.039	3.073	21
Q 1206+1500	2.60	1.793	2.568	4
Q 1206+1727	2.36	1.634	2.321	4
Q 1206+459	1.1580	0.4231	0.6300	3
Q 1206+459	1.1580	0.8426	1.1364	3
Q 1209+1046	2.20	1.634	2.163	4
Q 1209+1524	3.06	1.634	3.021	4
Q 1211+143	0.0850	0.0080	0.0742	3
Q 1212+1551	1.95	1.665	1.918	4
Q 1212+1045	1.95	1.634	1.922	4
Q 1212+0854	2.35	1.634	2.319	4
Q 1213+1015	2.52	1.634	2.482	4
Q 1213+0922	2.72	1.675	2.681	4
Q 1215+1244	2.08	1.634	2.048	4
Q 1215+1202	2.83	1.634	2.788	4
Q 1215+303	0.2370	0.0080	0.2246	3
Q 1216+069	0.3340	0.0080	0.3207	3
Q 1216+1517	1.83	1.723	1.802	4
Q 1216+1754	1.81	1.634	1.781	4
Q 1216+1656	2.83	1.659	2.791	4
Q 1216+0947	2.31	1.645	2.279	4
Q 1217+023	0.2400	0.0080	0.2276	3
Q 1218+304	0.1300	0.0080	0.1187	3

Table B1 – *continued*

Quasar	$z_{\rm em}$	$z_{\rm min}$	$z_{\rm max}$	Ref[a]
Q 1219+755	0.0700	0.0080	0.0593	3
Q 1219+1140	2.18	1.634	2.147	4
Q 1222+228	2.0400	0.4647	0.6316	3
Q 1222+1053	2.30	1.641	2.263	4
Q 1223+1059	2.32	1.643	2.288	4
Q 1223+1723	2.42	1.659	2.386	4
Q 1224+1244	2.14	1.634	2.110	4
Q 1225+1512	2.01	1.797	1.977	4
Q 1225+1610	2.23	1.663	2.200	4
Q 1225+317	2.2190	1.1263	1.5500	3
Q 1226+1035	2.32	1.634	2.287	4
Q 1226+1115	1.98	1.634	1.950	4
Q 1226+1639	2.25	1.634	2.216	4
Q 1226+023	0.1580	0.0080	0.1464	3
Q 1227+1215	2.17	1.624	2.138	4
Q 1228+1808	2.64	1.780	2.607	4
Q 1228+077	2.39	1.691	2.354	16
Q 1229+1414	2.90	1.764	2.862	4
Q 1229+1531	2.27	1.634	2.237	4
Q 1229−021	1.0380	0.4738	0.6320	3
Q 1229+204	0.0640	0.0080	0.0534	3
Q 1230+1042	2.43	1.634	2.396	4
Q 1230+1318	2.29	1.634	2.257	4
Q 1230+1627B	2.70	1.634	2.663	4
Q 1230+0941	1.84	1.641	1.812	4
Q 1232−0051	2.78	1.782	2.745	4
Q 1232+1139	2.87	1.848	2.831	4
Q 1234+0122	2.03	1.634	1.996	4
Q 1235+1807A	2.41	1.782	2.371	4
Q 1236−0043	1.84	1.690	1.815	4
Q 1236−0207	2.25	1.729	2.213	4
Q 1237+1515	2.04	1.634	2.009	4
Q 1237+0107	1.81	1.733	1.780	4
Q 1237+1508	2.07	1.634	2.035	4
Q 1237+1212	2.31	1.634	2.281	4
Q 1239+1435	1.93	1.634	1.900	4
Q 1239+0249	2.22	1.719	2.184	4
Q 1240+1504	1.85	1.634	1.823	4
Q 1241+176	1.2730	0.4066	0.6320	3
Q 1241+176	1.2730	0.7657	1.2503	3
Q 1242+0213	1.99	1.634	1.958	4
Q 1242+0006	2.08	1.634	2.045	4
Q 1242+1732	1.83	1.696	1.805	4
Q 1242+1737	1.86	1.634	1.828	4
Q 1244+1129	3.16	2.101	3.118	4
Q 1244+1642	2.87	1.848	2.826	4
Q 1246−0059	2.45	1.669	2.415	4
Q 1246+0032	2.31	1.651	2.273	4
Q 1247+267	2.0380	0.9211	1.5500	3
Q 1248+401	1.0300	0.3984	0.6028	3
Q 1248+401	1.0300	0.8919	1.0097	3
Q 1253−055	0.5380	0.0080	0.5226	3
Q 1259+593	0.4720	0.0080	0.4573	3
Q 1302−102	0.2860	0.0080	0.2731	3
Q 1307+085	0.1550	0.0080	0.1435	3
Q 1308+326	0.9960	0.4670	0.6310	3
Q 1308−0214	2.85	1.892	2.811	4
Q 1308−0104	2.59	1.634	2.549	4
Q 1309+355	0.1840	0.0080	0.1722	3
BR J1310−1740	4.185	2.508	4.133	26
Q 1312+043	2.35	1.813	2.319	16
Q 1313+0107	2.39	1.647	2.359	4
PSS J1317+3531	4.365	2.978	4.311	1
Q 1317+277	1.0220	0.2503	1.0018	3

Table B1 – *continued*

Quasar	$z_{\rm em}$	$z_{\rm min}$	$z_{\rm max}$	Ref[a]
Q 1318+290B	0.5490	0.3757	0.5335	3
Q 1318−0150	2.01	1.651	1.980	4
Q 1318−113	2.3080	1.896	2.273	16
Q 1320+0048	1.96	1.655	1.925	4
Q 1323−0248	2.12	1.661	2.090	4
Q 1324−0212	1.89	1.634	1.857	4
Q 1327−206	1.1690	1.1243	1.1473	3
Q 1328+0223	2.15	1.937	2.122	4
BRI B1328−0433	4.217	2.24	4.165	22
Q 1329+0231	2.43	1.663	2.400	4
Q 1329+0018	2.35	1.661	2.318	4
Q 1329+4117	1.9350	0.4853	0.6318	3
Q 1331+170	2.0840	1.2621	1.5500	3
Q 1333+176	0.5540	0.3902	0.5385	3
Q 1334+246	0.1070	0.0080	0.0959	3
Q 1334−0033	2.78	1.634	2.745	4
Q 1334+0212	2.38	1.634	2.350	4
BRI B1335−0417	4.396	3.08	4.342	22
Q 1336+0210	1.96	1.634	1.932	4
GB 1338+3809	3.10	1.737	3.059	2
Q 1338+101	2.45	1.724	2.412	16
Q 1338+416	1.2190	0.4066	0.6324	3
Q 1338+416	1.2190	0.8684	1.1968	3
Q 1340+0959	2.942	1.894	2.897	21
Q 1344+0137	1.92	1.634	1.886	4
Q 1345−0137	1.93	1.634	1.900	4
Q 1345−0120	2.95	1.926	2.906	4
Q 1346+0121A	1.93	1.634	1.901	4
Q 1346−036	2.36	1.653	2.327	16
Q 1351+640	0.0880	0.0080	0.0771	3
Q 1352+183	0.1520	0.0080	0.1405	3
Q 1352+108	3.18	1.928	3.137	16
Q 1353+186	0.0505	0.0080	0.0400	3
Q 1354+195	0.7200	0.3593	0.6330	3
Q 1355−416	0.3130	0.0080	0.2999	3
Q 1356+581	1.3710	0.5218	0.6310	3
Q 1358+115	2.59	1.677	2.550	16
Q 1358+3908	3.3	2.221	3.237	21
Q 1400+0935	2.980	2.022	2.930	21
Q 1402−012	2.52	1.789	2.479	16
Q 1402+044	3.20	2.340	3.160	16
Q 1406+123	2.94	2.018	2.903	16
Q 1407+265	0.9440	0.0080	0.9246	3
Q 1410+096	3.21	2.099	3.169	16
FIRST J1410+3409	4.351	3.026	3.578	26
		3.602	4.297	26
Q 1411+442	0.0900	0.0080	0.0791	3
GB 1413+3720	2.36	1.735	2.326	2
Q 1415+451	0.1140	0.0080	0.1029	3
Q 1416−129	0.1290	0.0080	0.1177	3
Q 1418+546	0.1520	0.0080	0.1405	3
Q 1419+480	0.0720	0.0080	0.0613	3
Q 1421+330	1.9040	1.0311	1.5500	3
Q 1425+267	0.3620	0.2409	0.3484	3
Q 1426+015	0.0860	0.0080	0.0751	3
Q 1428+0202	2.11	1.634	2.075	4
Q 1429−0053	2.08	1.719	2.047	4
Q 1429+118	3.00	1.958	2.963	16
PSS J1430+2828	4.306	2.777	4.253	1
Q 1433+0223	2.14	1.634	2.111	4
Q 1433−0025	2.04	1.634	2.012	4
PSS J1435+3057	4.297	2.905	4.244	1
GB 1436+4431	2.10	1.769	2.069	2
Q 1439+0047	1.86	1.649	1.828	4

Table B1 – *continued*

Quasar	z_{em}	z_{min}	z_{max}	Ref[a]
Q 1440−0024	1.81	1.634	1.786	4
Q 1440+356	0.0781	0.0080	0.0673	3
Q 1444+407	0.2670	0.0080	0.2543	3
Q 1444+0126	2.21	1.717	2.174	4
Q 1444−0112	2.15	1.651	2.121	4
Q 1451−375	0.3140	0.0080	0.3009	3
Q 1455+123	3.08	1.830	3.033	16
PSS J1456+2007	4.249	2.878	4.197	26
MG 1500+0431	3.67	2.606	3.623	1
Q 1503+118	2.78	1.957	2.740	16
GB 1508+5714	4.283	2.73	4.230	22
Q 1512+370	0.3710	0.0080	0.3573	3
MG 1519+1806	3.06	1.955	3.019	2
GB 1520+4347	2.18	1.775	2.148	2
Q 1522+101	1.3210	0.0080	0.6310	3
Q 1522+101	1.3210	0.8803	1.2978	3
Q 1525+227	0.2530	0.0080	0.2405	3
GB 1526+6701	3.02	1.955	2.980	2
Q 1526+285	0.4500	0.0080	0.2428	3
Q 1538+477	0.7700	0.3326	0.6326	3
Q 1545+210	0.2640	0.0080	0.2514	3
Q 1548+0917	2.749	1.874	2.707	21
PC 1548+4637	3.544	2.607	3.499	1
Q 1553+113	0.3600	0.0080	0.3464	3
Q 1556+273	0.0899	0.0080	0.0790	3
MG 1557+0313	3.891	2.66	3.842	22
MG 1559+1405	2.24	1.737	3.059	2
Q 1600+0729	4.38	3.062	4.326	1
BR J1603+0721	4.385	3.062	4.331	26
Q 1607+1819	3.123	1.814	3.0918	21
Q 1612+261	0.1310	0.0080	0.1197	3
Q 1613+658	0.1290	0.0080	0.1177	3
Q 1623+268A	2.47	1.644	2.433	16
Q 1623+268B	2.54	1.644	2.502	16
Q 1630+377	1.4710	0.0080	0.6320	3
Q 1630+377	1.4710	0.8641	1.4463	3
Q 1631+3722	2.940	1.785	2.906	21
PSS J1633+1411	4.351	2.536	4.297	26
Q 1634+706	1.3340	0.5547	1.3107	3
Q 1641+399	0.5950	0.0080	0.5791	3
PC 1640+4628	3.700	2.604	3.653	1
PSS J1646+5514	4.037	2.772	3.987	26
Q 1704+608	0.3710	0.0080	0.3573	3
Q 1705+0152	2.576	1.669	2.537	21
Q 1715+535	1.9290	1.1009	1.5500	3
Q 1718+481	1.0840	0.0080	1.0632	3
PSS J1721+3256	4.031	2.791	3.981	26
Q 1721+343	0.2060	0.0080	0.1939	3
Q 1726+3425	2.429	1.669	2.393	21
Q 1727+502	0.0550	0.0080	0.0445	3
Q 1738+3502	3.240	2.093	3.197	21
GB 1745+6227	3.901	2.47	3.852	22
Q 1803+676	0.1360	0.0080	0.1246	3
Q 1807+698	0.0512	0.0080	0.0407	3
Q 1821+643	0.2970	0.0080	0.2840	3
Q 1831+731	0.1230	0.0080	0.1118	3
Q 1833+326	0.0590	0.0080	0.0484	3
Q 1836+5108	2.827	1.920	2.789	21
Q 1839−785	0.0743	0.0080	0.0636	3
Q 1845+797	0.0556	0.0080	0.0450	3
Q 1912−550	0.4020	0.1769	0.2041	3
Q 1928+738	0.3020	0.0080	0.2890	3

Table B1 – *continued*

Quasar	z_{em}	z_{min}	z_{max}	Ref[a]
PKS 1937−101	3.787	2.442	3.739	21
Q 2000−3300	3.783	2.521	3.729	21
Q 2005−489	0.0710	0.0080	0.0603	3
Q 2038−0116	2.783	1.887	2.745	21
Q 2045−377	1.8000	1.0040	1.5500	3
Q 2048+3116	3.198	1.830	3.143	21
Q 2050−359	3.49	2.605	3445	1
Q 2112+0555	0.4660	0.1105	0.4513	3, 24, 25
Q 2113−4345	2.05	1.664	2.023	4
Q 2113−4534	2.54	1.969	2.506	4
Q 2114−4346	2.04	1.606	2.011	4
Q 2115−4434	2.16	1.755	2.128	4
Q 2117−4703	2.26	1.849	2.223	4
Q 2122−4231	2.27	1.550	2.233	4
Q 2126−1551	3.2660	2.011	3.218	21
Q 2126−4618	1.89	1.715	1.859	4
Q 2127−4528	2.71	2.018	2.676	4
Q 2128−123	0.5010	0.0940	0.4860	3
Q 2130+099	0.0610	0.0080	0.0504	3
Q 2131−4257	2.10	1.590	2.065	4
PMN J2134−0419	4.334	2.903	4.281	26
Q 2134−4239	1.80	1.590	1.776	4
Q 2134−147	0.2000	0.0080	0.1880	3
Q 2135−4632	2.21	1.879	2.182	4
Q 2136+141	2.43	1.784	2.390	16
Q 2139−4434	3.23	2.373	3.188	4
Q 2141+175	0.2130	0.0080	0.2009	3
Q 2145+067	0.9900	0.9426	0.9701	3
MG 2152+1420	2.56	1.800	2.524	2
Q 2153−2056	1.85	1.634	1.821	4
Q 2155−304	0.1170	0.0080	0.1058	3
Q 2159−2058	2.12	1.634	2.089	4
Q 2201+315	0.2970	0.0080	0.2840	3
Q 2203−2145	2.27	1.692	2.240	4
Q 2203−1833	2.73	1.849	2.691	4
Q 2205−2014	2.64	1.652	2.599	4
MG 2206+1753	3.14	1.769	3.099	2
Q 2209−1842	2.09	1.634	2.061	4
Q 2209+184	0.0700	0.0080	0.0593	3
Q 2211−1915	1.95	1.634	1.923	4
BR B2212−1626	3.990	2.69	3.940	22
Q 2214+139	0.0658	0.0080	0.0551	3
BR J2216−6714	4.469	2.795	4.414	26
MG 2222+0511	2.32	1.800	2.287	2
GB 2223+2024	3.56	2.101	3.514	2
Q 2231+0125	1.90	1.634	1.871	4
Q 2231−0212	1.90	1.634	1.871	4
Q 2233+1341	3.209	2.216	3.167	21
Q 2233+1310	3.298	2.134	3.252	21
Q 2241+0014	2.14	1.657	2.099	4
Q 2243+0141	2.30	1.663	2.267	4
Q 2244−0234	1.97	1.787	1.940	4
Q 2244−0105	2.04	1.634	2.010	4
Q 2246−0006	2.05	1.651	2.019	4
BR B2248−1242	4.161	2.94	4.109	22
MG 2251+2429	2.33	2.019	2.297	2
Q 2251−178	0.0680	0.0080	0.0573	3
Q 2251+113	0.3230	0.1310	0.3098	3
MG 2254+0227	2.09	2.767	2.059	2
Q 2256+017	2.67	1.786	2.629	16
Q 2302+029	1.0440	0.3942	0.6290	3
Q 2302+029	1.0440	0.8060	1.0236	3

Table B1 – *continued*

Quasar	$z_{\rm em}$	$z_{\rm min}$	$z_{\rm max}$	Ref[a]
Q 2308+098	0.4320	0.0080	0.4177	3
Q 2311−0341	3.048	1.714	3.001	21
MG 2320+0755	2.09	1.780	2.059	2
Q 2326−477	1.2990	0.9164	1.2760	3
BR J2328−4513	4.359	2.926	4.305	26
PC 2331 + 0216	4.093	3.115	4.042	1
Q 2334+1041	2.243	1.634	2.211	21
Q 2344+092	0.6720	0.0080	0.6288	3
BR J2349−3712	4.208	2.847	4.156	26
Q 2351+1042	2.379	1.632	2.345	21
Q 2351+0120	2.07	1.634	2.039	4
Q 2351−1154	2.67	1.632	2.633	21
Q 2352+0205	2.19	1.634	2.158	4
Q 2354−0134	2.21	1.665	2.178	4
Q 2356+0139	2.07	1.661	2.039	4
Q 2356+0237	2.50	1.634	2.465	4

Table B1 – *continued*

Quasar	$z_{\rm em}$	$z_{\rm min}$	$z_{\rm max}$	Ref[a]
Q 2359+0653	3.238	1.632	3.203	21
Q 2359+0023	2.897	1.714	2.857	21

[a]References: (1) Storrie-Lombardi & Wolfe (2000); (2) Storrie-Lombardi & Hook (2000); (3) Lanzetta et al. (1995); (4) Wolfe et al. (1995); (5) Sargent et al. (1989); (6) Turnshek et al. (1989); (7) Wolfe et al. (1993); (8) Lu et al. (1993); (9) Lu & Wolfe (1994); (10) Virgilio et al. (1995); (11) Pettini et al. (1994); (12) Francis & Hewett (1993); (13) Savaglio et al. (1994); (14) Sargent et al. (1988); (15) Black et al. (1987); (16) Wolfe et al. (1986); (17) Wolfe et al. (1994); (18) Rauch et al. (1990); (19) Williger et al. (1989); (20) Meyer et al. (1995); (21) Lanzetta et al. (1991); (22) Storrie-Lombardi et al. (1996c); (23) Storrie-Lombardi et al. (1996a); (24) Jannuzi et al. (1998); (25) Fynbo et al. (2001); (26) Péroux et al. (2001).

This paper has been typeset from a TEX/LATEX file prepared by the author.